



# Hazards of decreasing marine oxygen: the near-term and millennial-scale benefits of meeting the Paris climate targets

Gianna Battaglia<sup>1,2</sup> and Fortunat Joos<sup>1,2</sup>

<sup>1</sup>Climate and Environmental Physics, Physics Institute, University of Bern, Bern, Switzerland

<sup>2</sup>Oeschger Centre for Climate Change Research, University of Bern, Bern, Switzerland

Correspondence to: Gianna Battaglia ([battaglia@climate.unibe.ch](mailto:battaglia@climate.unibe.ch))

**Abstract.** Ocean deoxygenation is recognized as key ecosystem stressor of the future ocean and associated climate-related ocean risks are relevant for policy decisions today. In particular, benefits of reaching the ambitious 1.5 °C warming target mentioned by the Paris Agreement compared to higher temperature targets are of high interest. Here, we model oceanic oxygen, warming, and their compound hazard in terms of metabolic conditions on multi-millennial timescales for a range of temperature targets. Scenarios, where radiative forcing is stabilized by 2300, are used in ensemble simulations with the Bern3D Earth System Model of Intermediate Complexity. Transiently, the global mean ocean oxygen concentration decreases by a few percent under low and by 40 % under high forcing. Deoxygenation peaks about thousand years after stabilization of radiative forcing. Hypoxic waters expand over the next millennium and recovery is slow and remains incomplete under high forcing. Largest transient decreases in oxygen are projected for the deep sea. Distinct and close to linear relationships between the equilibrium temperature response and marine O<sub>2</sub> loss emerge. These point to the effectiveness of the Paris climate target in reducing marine hazards and risks. Mitigation measures are projected to reduce peak decreases in oceanic oxygen inventory by 4.4 % °C<sup>-1</sup> of avoided equilibrium warming. In the upper ocean, the decline of a metabolic index, quantified by the ratio of O<sub>2</sub> supply to an organism's O<sub>2</sub> demand, is reduced by 6.2 % °C<sup>-1</sup> of avoided equilibrium warming. Measures of peak hypoxia exhibit a strong sensitivity to additional warming. Volumes of water with less than 50 mmol O<sub>2</sub> m<sup>-3</sup>, for instance, increase between 36 % to 76 % °C<sup>-1</sup> of equilibrium temperature response. Our results show that millennial-scale responses should be considered in assessments of ocean deoxygenation and associated climate-related ocean risks. Peak hazards occur long after stabilization of radiative forcing and new steady state conditions establish after AD 8000.

## 1 Introduction

Several key marine and coastal ecosystems are recognized to face high risk of impact due to climate change even if low emissions pathways are followed to the end of the century (*Gattuso et al., 2015; Magnan et al., 2016*). The most prominent marine ecosystem stressors include warming, acidification, deoxygenation, hypocapnia, changes in food supply and sea-level rise (*Gruber, 2011; Cocco et al., 2013; Bopp et al., 2013; Gattuso et al., 2015; Sweetman et al., 2017*). Risks arise both from changes in mean environmental conditions in response to climate change and potential changes in the frequency and severity of extreme events. This growing body of concern contributed to motivate the 21st Conference of the Parties (COP21) to reach the



Paris Agreement with the goal of keeping the global mean atmospheric temperature rise by the end of the 21st century to well below 2 °C, if not below 1.5 °C, above preindustrial (Magnan *et al.*, 2016; UNFCCC, accessed 11. October 2017). It is now a  
5 key scientific task to further assess what the impacts of global warming of 1.5-2 °C are on the ocean, not just by the end of the 21st century but on the typical equilibration timescale of the ocean which spans several millennia. Here we consider potential changes in oceanic oxygen and the hazard of hypoxia across a range of warming targets over the next 8000 years within the Bern3D Earth System Model of Intermediate Complexity (EMIC).

Oxygen (O<sub>2</sub>) is a sparingly soluble gas and its distribution in the ocean results from the sum of its solubility component  
10 set through air-sea exchange, the effect of O<sub>2</sub> production by phytoplankton in the euphotic zone and O<sub>2</sub> consumption during organic matter remineralization at depth. Typical thresholds for hypoxia are approximately 50 mmol m<sup>-3</sup>. Water with lower O<sub>2</sub> concentrations are effectively dead zones for many higher animals (reviewed in Keeling *et al.*, 2010; Storch *et al.*, 2014). Species are also sensitive to thermal stress (Gattuso *et al.*, 2015) and their sensitivity to hypoxia increases with higher temperatures (Pörtner, 2010). In the modern ocean, oxygen-poor zones with O<sub>2</sub> < 50 mmol m<sup>-3</sup> occupy about 5 % of its volume (Garcia  
15 *et al.*, 2014; Bianchi *et al.*, 2012). Expanding oxygen-poor waters lead to habitat compression, mortality and major changes in community structure where energy preferentially flows into microbial pathways to the detriment of higher trophic levels. Suboxia can also lead to production of poisonous H<sub>2</sub>S within sediments (reviewed in Diaz and Rosenberg, 2008).

Observational (Schmidtko *et al.*, 2017; Ito *et al.*, 2017) and modeling studies (Oschlies *et al.*, 2017) indicate an overall  
20 decline in the oceanic oxygen content over past decades. Systematic discrepancies exist for the typically low oxygen tropical thermocline, where observations suggest O<sub>2</sub> has decreased and most models simulate increased O<sub>2</sub> levels over the past decades. Model projections to the end of the 21st century consistently project the global ocean oxygen inventory to further decline (Matear, 2000; Plattner *et al.*, 2001; Bopp *et al.*, 2002; Frölicher *et al.*, 2009; Cocco *et al.*, 2013; Bopp *et al.*, 2013). Impact studies have highlighted potential habitat compression (Deutsch *et al.*, 2015; Mislán *et al.*, 2017) and reduced catch potential (Cheung *et al.*, 2016) associated with climate change at the end of the century. Large model-model differences remain in  
25 projections of oxygen minimum zones (OMZs) (Cocco *et al.*, 2013; Bopp *et al.*, 2013).

The geologic record provides additional insight into sensitivities to climate change, even though the current increase in radiative forcing is more than an order of magnitude faster than any sustained change during the past 22,000 years (Joos and Spahni, 2008). Oxygenation proxies reveal changes in oxygen for millennial scale processes and between glacial-interglacial transitions due to changes in ocean circulation and mixing, changes in oxygen consumption and solubility. For instance, atmospheric CO<sub>2</sub> and abyssal Southern Ocean oxygenation co-varied throughout the past 80,000 years reflecting enhanced deep  
30 ocean ventilation and less iron fertilization (Jaccard *et al.*, 2016). Also, abrupt warming events in the past have been shown to coincide with sudden appearance of hypoxia at intermediate depths in the North Pacific (Praetorius *et al.*, 2015) raising concern for impacts in the future. Across the last deglaciation, the deep ocean became better oxygenated and low oxygen water in the upper ocean expanded as the Earth transitioned to a warm interglacial state, opposite the general expectation from a pure solubility point of view (Jaccard and Galbraith, 2012; Jaccard *et al.*, 2014). Earth System projections to the end of the  
35 21st century are showing decreases in oxygen with warming and are therefore apparently in conflict with this geologic sense



of change. Nevertheless, these simulations represent transient climate states and long term simulations are required for more adequate comparisons to past climate states.

Here, we employ 4x100-member ensemble simulations with the Bern3D model run to year AD 10,000 by which time the ocean has reached new steady state conditions. Radiative forcing is prescribed to stabilize by 2300 and four different temperature targets are considered (1.5, 1.9, 3.3 and 9.2 °C above preindustrial). Each ensemble recognizes uncertainties in critical parameters of mixing and remineralization. We evaluate the response in oceanic oxygen content and a number of additional ecosystem stressors including warming, export production and a metabolic index. Oxygen changes arising from different contributions (production, consumption, solubility) are explicitly traced such that changes can be attributed to processes. We focus the description of spatial changes on the 1.5 °C warming target, the ambitious target mentioned by the Paris Agreement. Avoided hazards compared to higher temperature targets are evaluated at the global scale. A range of multi-millennial projections available so far have focused primarily on the evolution of surface air temperature (SAT), atmospheric CO<sub>2</sub>, oceanic pH, sea level and the Atlantic Meridional Overturning Circulation (AMOC) (*Plattner et al.*, 2008; *Eby et al.*, 2009; *Zickfeld et al.*, 2013; *Golledge et al.*, 2015; *Winkelmann et al.*, 2015; *Clark et al.*, 2016; *Zickfeld et al.*, 2017; *Pfister and Stocker*, 2016; *Lord et al.*, 2016; *Ehlert and Zickfeld*, 2017). Fewer long-term model simulations have focused on oceanic oxygen (*Yamamoto et al.*, 2015; *Matear and Hirst*, 2003; *Schmittner et al.*, 2008; *Mathesius et al.*, 2015). We show that the oceanic oxygen equilibration timescale is considerably longer than its thermal equilibration timescale and that oceanic oxygen changes are dominated by changes in Atlantic and Indo-Pacific overturning, predictive variables to be considered in future multi-millennial projections with General Circulation Models (GCMs). We also highlight that a full account of climate-related ocean risks should include long-term, multi-millennial perspectives as most severe hazards occur long after stabilization of radiative forcing and the reduction of anthropogenic carbon emissions.

## 2 Model and Simulations

### 2.1 Bern3D

The Bern3D Earth System Model of Intermediate Complexity is a three dimensional frictional geostrophic balance ocean model (*Müller et al.*, 2006), which includes a sea ice component coupled to a single-layer energy and moisture balance model of the atmosphere (*Ritz et al.*, 2011) and a prognostic marine biogeochemistry module (*Tschumi et al.*, 2011; *Parekh et al.*, 2008). A version with 41x40 horizontal grid-cells and 32 vertical layers is used (see also *Roth et al.*, 2014; *Battaglia et al.*, 2016 for model evaluation). The NCEP/NCAR monthly wind-stress climatology (*Kalnay et al.*, 1996) is prescribed at the surface. Air-sea gas exchange, carbonate chemistry and natural  $\Delta^{14}\text{C}$  of DIC is modeled according to OCMIP-2 protocols (*Najjar et al.*, 1999; *Orr and Najjar*, 1999; *Orr and Epitalon*, 2015). The global mean air-sea transfer rate is reduced by 19 % compared to OCMIP-2 to match observation-based estimates of natural and bomb-produced radiocarbon (*Müller et al.*, 2008).

The biogeochemical module is based on phosphorus and simulates production and remineralization/dissolution of organic matter, calcium carbonate and opal. Production of particulate organic matter (POP) within the euphotic zone (top 75 m) depends on temperature, light availability, phosphate and iron following *Doney et al.* (2006). POP remineralization within the water



column follows a power law profile (*Martin et al.*, 1987). Organic matter falling on to the sea floor is remineralized in the deepest box. Two thirds of organic matter production form dissolved organic matter (DOP), which decays with an e-folding lifetime of 1.5 years. An updated remineralization scheme assigns remineralization of POP and DOP to aerobic and anaerobic pathways depending on the mean grid-cell dissolved O<sub>2</sub> concentration (see *Battaglia and Joos* (2017)). We introduce two power law profiles with two distinct remineralization length scales for aerobic and anaerobic remineralization ( $\alpha_{\text{aerob}}$  and  $\alpha_{\text{denit}}$ ). Constant stoichiometric ratios are used for both aerobic and anaerobic remineralization to convert biological P fluxes into carbon, and alkalinity fluxes (P:Alk:C=1:17:117). The O<sub>2</sub> demand for complete aerobic remineralization is  $170 \frac{\text{molO}_2}{\text{molPO}_4}$  and no oxygen is consumed for anaerobic remineralization. Accordingly, aerobic remineralization in the ocean is smaller than O<sub>2</sub> production in the euphotic zone leading to an O<sub>2</sub> outgassing for steady state conditions. The atmospheric oxygen inventory is constant. This is justified as 99.5 % of the ocean-atmosphere inventory is in the atmosphere and potential net fluxes of O<sub>2</sub> from the ocean and land to the atmosphere and fossil fuel burning have a small impact on atmospheric O<sub>2</sub>. O<sub>2</sub> components from O<sub>2</sub> production, consumption and solubility are carried as explicit model tracers to attribute changes. Tracers add up to within 10<sup>-14</sup> Pmol with mean inventories of 23.2, -239.3, 429.9 yielding a total of 213.5 Pmol, respectively (median values given).

We include evaluation of a metabolic index,  $\Phi$ , which was proposed by *Deutsch et al.* (2015). It combines temperature and pO<sub>2</sub> as indicators of metabolically viable environments and is defined as the ratio of O<sub>2</sub> supply to an organism's resting O<sub>2</sub> demand. We consider only relative changes in  $\Phi(t)$  relative to a reference time,  $t_0$  (average over 1870-1899):

$$\frac{\Delta\Phi(t)}{\Phi(t_0)} = \frac{pO_2(t)}{pO_2(t_0)} \times \exp\left(\frac{E_0}{k_B} \left(\frac{1}{T(t)} - \frac{1}{T(t_0)}\right)\right) - 1, \quad (1)$$

where  $T$  is the absolute temperature,  $k_B$  is Boltzmann's constant and the exponential function and the parameter  $E_0$  characterize the temperature dependence of the baseline metabolic rate.  $E_0$  only weakly affects the relative influence of temperature and O<sub>2</sub> gradients and relative changes in  $\Phi$  are therefore independent on species (*Deutsch et al.*, 2015). Here, we consider  $E_0=0.87$  (representative of Atlantic cod). For the calculation of  $pO_2$  we pressure-correct the equilibrium constant following Eq. 5 in *Weiss* (1974).

The current set up does not include sediment interactions, temperature dependent remineralization, variable stoichiometry, nitrogen-cycle feedbacks, atmospheric nutrient deposition, dynamic wind nor freshwater input/albedo changes from melting of continental ice-sheets.

## 2.2 Ensemble and scenarios

To explore potential oxygen changes we set up four 100-member ensembles each targeting a different equilibrium temperature response ( $\sim 1.5, 1.9, 3.3$  and  $9.2$  °C above preindustrial). A feedback parameter  $\lambda$  [ $\text{W m}^{-2} \text{K}^{-1}$ ] (*Ritz et al.*, 2011), accounting for climate feedbacks that are not explicitly treated in the Bern3D model, is chosen in combination with radiative forcing from the Representative Concentration Pathways (RCPs) (*Meinshausen et al.*, 2011) to achieve these stabilization targets. RCP2.6, stabilizing by 2300, is run with  $\lambda$  values of -0.71 and  $-1 \text{ W m}^{-2} \text{K}^{-1}$  achieving the 1.5 and 1.9 °C targets, respectively. RCP4.5,



stabilizing after 2100, is run with  $-1 \text{ W m}^{-2} \text{ K}^{-1}$  yielding a  $3.3 \text{ }^\circ\text{C}$  temperature response and RCP8.5, stabilizing in the 23rd century, with  $-0.71 \text{ W m}^{-2} \text{ K}^{-1}$  yielding a  $9.2 \text{ }^\circ\text{C}$  response (median values given for temperature targets). Each member is spun up over 5000 years to AD 1765 boundary conditions. The radiative forcing follows RCP scenarios (RCP2.6, 4.5 and 8.5, *Meinshausen et al.*, 2011). The RCP scenarios are extended to year AD 10,000 by which time the ocean has equilibrated to new steady state conditions. Radiative forcing includes an 11-year solar cycle up to year AD 3000. After that, all forcings are kept constant. We employ a single-model setup, and assess uncertainties arising from organic matter remineralization ( $\alpha_{\text{aerob}}$  and  $\alpha_{\text{denit}}$ ) and vertical mixing ( $k_{\text{diff-dia}}$ ). The three parameters are sampled using the Latin Hypercube sampling technique (*McKay et al.*, 1979). The parameter ranges are chosen such that all members achieve similar skill scores with respect to observation-derived fields of natural radiocarbon (*Key et al.*, 2004) and dissolved  $\text{O}_2$  (*Garcia et al.*, 2014; *Bianchi et al.*, 2012) and correspond to the values chosen in *Battaglia and Joos* (2017).

### 2.3 Pre-Industrial characteristics

The ensemble produces a range in overturning strengths, remineralization fluxes and  $\text{O}_2$  distributions. The following numbers represent the 90 % confidence ranges of important model characteristics across the ensemble. The AMOC ranges from 16.5 to 19.7 Sv, Indo-Pacific meridional overturning (Indo-Pacific MOC) ranges between -13.6 to -15.6 Sv and export of particulate organic matter from 9.0 to 11.4 Gt C  $\text{yr}^{-1}$ . The simulated oxygen inventory ranges between 195 and 230 Pmol given the three parameters and the simulated oxygen distribution covers the observational range well (Fig. 7a in *Battaglia and Joos*, 2017). Biases exist in the simulated extend of OMZs. The volume of suboxic conditions ( $\text{O}_2 < 5 \text{ mmol m}^{-3}$ ) is overestimated by a factor of five but water column denitrification fluxes are well within current estimates (Table C.1., Fig. 2c in *Battaglia and Joos*, 2017). This is a common model bias in EMICs and GCMS (*Cocco et al.*, 2013; *Bopp et al.*, 2013; *Cabre et al.*, 2015). Vastly enhanced spatial resolution may be required to simulate equatorial physics and ecosystems in better agreement with observations (*Bopp et al.*, 2013).

### 3 Peak oxygen decreases scale linearly with forcing

We first explore how oxygen changes scale with forcing at different timescales (Fig. 1 and 2). In response to the RCP scenarios, atmospheric temperatures rise and stabilize after  $\sim 1000$  years (Fig. 2a). The response in oceanic oxygen is more complex and characterized by an initial decline followed by a recovery phase (Fig. 2b). Our results demonstrate the potential for large changes in marine oxygen under anthropogenic forcing, a large inertia in the response and a slow, and partially incomplete recovery of the perturbation. Transiently, the whole ocean oxygen inventory decreases by a few percent (6 %) under low forcing and by as much as 40 % under high forcing (median values given). The minimum in oxygen occurs about thousand years after stabilization of radiative forcing, and it takes several millennia to approach a new equilibrium. Then, the global ocean  $\text{O}_2$  inventory is a few percent higher than at preindustrial conditions under low and intermediate forcing and remains depleted by around 8 % in the high forcing case.



The magnitude of changes in  $O_2$  and related hazards generally increase with the magnitude of forcing and warming. Distinct and close to linear relationships between changes in SAT and in marine  $O_2$  emerge. Transient (end of 21st century), peak (AD  $\sim 3000$ ) and equilibrium (AD  $\sim 8000$ ) oxygen changes exhibit distinct relationships to their corresponding warming (Fig. 1a).

5 At the end of the 21st century, simulated oxygen decreases by  $0.68\% \text{ } ^\circ\text{C}^{-1}$  of realized warming (median values). At peak oxygen decline, this sensitivity increases and oxygen decreases by  $4.4\% \text{ } ^\circ\text{C}^{-1}$  of equilibrium temperature response. The linear relationship breaks down for the equilibrium response. While 1.5 to  $3.3\text{ } ^\circ\text{C}$  warming targets lead to similar and higher oxygen levels, the  $9.2\text{ } ^\circ\text{C}$  warming target results in lower oxygen levels compared to preindustrial. The sensitivities across different timescales are very similar across the parameter space. Lower mixing coefficients lead to larger decreases in absolute

10 terms.

The volume of low oxygen waters is particularly sensitive to warming and parameter uncertainty (Fig. 1b). We illustrate the sensitivities at the example of the volume of waters with  $O_2 < 50\text{ mmol m}^{-3}$ . At the end of the 21st century, there is a  $1.7\%$  increase in this volume per  $^\circ\text{C}$  of realized warming. Peak increases scale with  $63\% \text{ } ^\circ\text{C}^{-1}$  of equilibrium temperature response. Uncertainties in remineralization cause a spread in this response ranging from  $36\text{--}76\% \text{ } ^\circ\text{C}^{-1}$  of equilibrium temperature

15 response (90% confidence range): The deeper the remineralization length scale, the higher this sensitivity. Pre-existing low  $O_2$  waters expand and new low  $O_2$  waters may develop in near bottom environments for higher forcing levels. While the lower temperature targets yield lower volumes of low oxygen waters, the  $9.2\text{ } ^\circ\text{C}$  target yields higher low  $O_2$  volumes under new steady state conditions. In brief, hypoxic waters expand over the next millennium across the scenario range and recovery towards modern conditions is slow and in the case of high forcing incomplete.

20 Simulated changes in export, too, exhibit a distinct temporal evolution. Changes at the end of the 21st century scale with  $-1.2\% \text{ } ^\circ\text{C}^{-1}$  of realized warming and peak changes scale with  $-0.93\% \text{ } ^\circ\text{C}^{-1}$  of equilibrium temperature response. The global recovery level is similar among the forcings.

The metabolic index  $\Phi$ , as proposed by *Deutsch et al.* (2015), is linear in  $pO_2$  (representing the rate of  $O_2$  supply) and decreases non-linearly with temperature (indicative of the resting metabolic demand). The globally averaged, upper ocean

25 (depth  $< 400\text{ m}$ ) metabolic index declines throughout the simulation dominated by increased temperatures. Decreases scale linearly with forcing:  $5.1\% \text{ } ^\circ\text{C}^{-1}$  of realized warming at the end of the 21st century and  $6.2\% \text{ } ^\circ\text{C}^{-1}$  of equilibrium temperature response. Likewise, global mean oceanic temperatures increase by  $0.099\text{ } ^\circ\text{C } ^\circ\text{C}^{-1}$  of realized warming at the end of the 21st century and by  $0.56\text{ } ^\circ\text{C } ^\circ\text{C}^{-1}$  of equilibrium surface air temperature response. In conclusion, the compound hazards related to deoxygenation and warming, as indicated by the metabolic stress index, evolve over millennia and increase with increasing

30 anthropogenic forcing and with time.

Not only the magnitude or intensity, but also the duration of oxygen related, transient hazards, and thus the severity of the hazards increases with increasing temperature targets. The severity combines magnitude and duration of a hazard in one measure. It may be defined as the time integral of a hazard. The severity of the hazard of expanding hypoxic waters, for example, corresponds to the area under the scenario curve shown in Fig. 2i (the area enclosed by the null line and the modeled

35 evolution, here until the end of the simulation). Fig. 2b,h, and i illustrate that the severity of the three hazards decreasing mean



oxygen concentration, expanding hypoxic waters, and reduced export of particulate organic matter providing food for deep sea organisms, increases strongly from low to high temperature targets.

Figure 2 further explains the temporal evolution and interplay of the underlying drivers. In all cases, the changes in global oxygen inventory strongly correlate with water mass age and are also impacted by gradual oxygen loss due to warming (Fig. 2e,f). Inventory changes based on the O<sub>2</sub> production tracer are negligible; changes equilibrate with the atmosphere and only a small fraction remains in the ocean. The O<sub>2</sub> consumption tracer determines the shape of the global O<sub>2</sub> signal. It correlates strongly with ideal age and integrates changes in overturning and remineralization fluxes. Changes from remineralization fluxes include both changes in absolute aerobic remineralization fluxes and changes in the relative share of denitrification. An increased share of denitrification at organic matter remineralization, for instance, effectively constitutes an implicit O<sub>2</sub> gain. Denitrification fluxes correlate with the volumetric expansion of OMZs and are also impacted by changes in remineralization fluxes within them (Fig. 2j). O<sub>2</sub> loss due to warming adds to transient decreases in O<sub>2</sub> utilization and diminishes the recovery level. As such, 1.5 to 3.3 °C warming targets reach similar equilibrium levels for different reasons. The degree of increased overturning from additional warming and resulting oxygenation in relation to O<sub>2</sub> loss due to higher temperatures cancel out. The 9.2 °C warming target reaches a lower equilibrium inventory compared to preindustrial due to high O<sub>2</sub> loss from solubility (-44.1 Pmol).

The decline and recovery pattern in oxygen changes is dominated by changes in overturning. Both Atlantic and Indo-Pacific overturning are projected to slow down and recover. Decline and recovery level as well as the decline and recovery rate vary with forcing level. Generally, Bern3D projects larger slowdown for higher forcing (Fig. 2c,d). The recovery level with forcing differs among AMOC and Indo-Pacific MOC. Higher forcing levels tend to lead to lower recovery for the AMOC and higher recovery levels for the Indo-Pacific MOC. This has direct consequences for the projected global water mass age and by that for oceanic oxygen. The higher the forcing, the higher the transient increase in water mass age. The decrease in global water mass age, which is larger for higher forcing, is dominated by increased Indo-Pacific MOC.

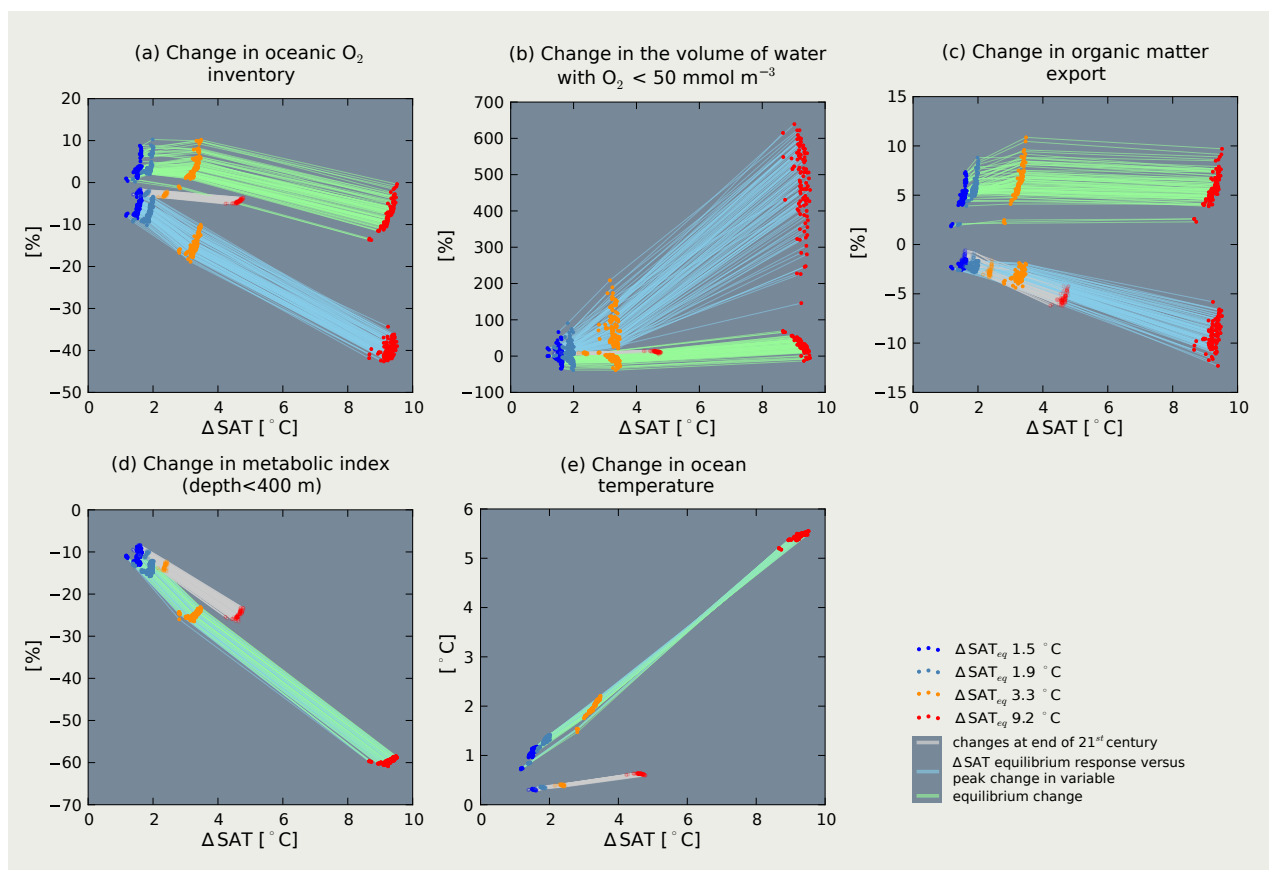


**Figure 1.** Changes in marine ecosystem stressors versus changes in global mean surface air temperature at three distinct points in time relative to 1870-1899. The colored dots indicate results of the four 100-member ensembles targeted to reach 1.5 (blue dots), 1.9 (light blue dots), 3.3 (orange dots) and 9.2  $^{\circ}\text{C}$  (red dots) warming targets. The lines connect results of individual ensemble members at 2100 AD (gray), at time of peak decline of each variable (light blue) and by the end of the simulation (light green) when a new equilibrium state has been reached. Peak and equilibrium changes in variables of interest are related to the corresponding equilibrium temperature response, while changes at the end of the 21st century are related to the transiently realized warming. Peak and equilibrium responses are indistinguishable in the figure for the metabolic index (d) and the ocean temperature change (e).



#### 4 Spatial changes in physical and biological variables for a 1.5 °C warming target

We now address spatial changes in critical variables for a single, representative ensemble member at its peak O<sub>2</sub> decline which occurs at year AD 3150 and amounts to 5 % (Fig. 3). The member eventually reaches a 1.5 °C warming target. O<sub>2</sub> changes show strong spatial correlation with changes in water mass age (Fig. 3a,b). Despite the global decrease, higher O<sub>2</sub> concentrations are simulated in subsurface waters where ideal age is younger. In near surface waters, local changes in remineralization may contribute to oxygen changes. Below 2 km, overall lower O<sub>2</sub> concentrations are simulated compared to preindustrial. Highest decreases are simulated in bottom waters in line with older water mass age. The presented gradients at peak O<sub>2</sub> decline tend to be more pronounced for higher forcings.

Export of particulate organic matter is simulated to increase in high latitudes and decrease elsewhere (Fig. 3c). Decreases in export production result from increased stratification and a concomitant increase in nutrient limitation in low latitudes (Fig. 3d, see also *Steinacher et al. (2009); Battaglia and Joos (2017)*). The increases in export production in the Arctic and Southern Ocean are due to less temperature and light limitation as surface waters warm and sea ice retreats.

The temperature anomaly is strongest within the upper ocean and decreases with depth. A pronounced temperature anomaly develops in the upper South Equatorial Atlantic Ocean (Fig. 3f).

The metabolic index,  $\Phi$  (*Deutsch et al., 2015*), decreases in most places in line with warming and lower pO<sub>2</sub>. The O<sub>2</sub> gain in upper ocean waters is able to counteract the adverse effect of warming in some high latitude environments. In other places with higher pO<sub>2</sub>, the temperature increase dominates the response in  $\Phi$ . Near bottom waters in the Pacific are prone to largest reductions in  $\Phi$ , driven by large decreases in pO<sub>2</sub>.

The equilibrium response in O<sub>2</sub> for this 1.5 °C warming case is characterized by slight O<sub>2</sub> decreases in the Atlantic, caused mainly by less solubility, and increases in the Southern Ocean and deep Pacific, caused by higher overturning and less sea-ice coverage in the Southern Ocean compared to preindustrial.

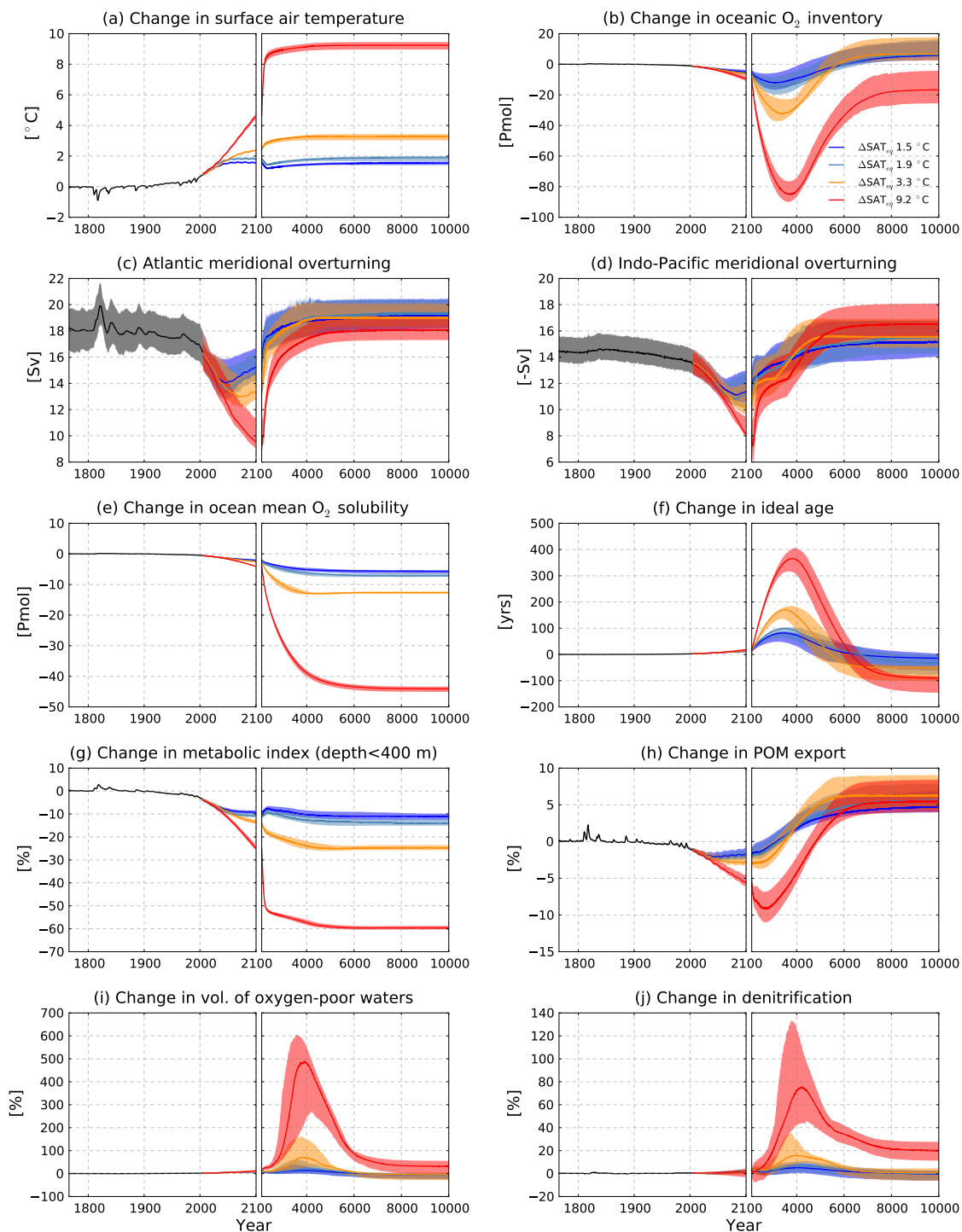


**Figure 2.** Temporal evolution of critical variables relative to 1870-1899 for the model ensembles aiming at 1.5, 1.9, 3.3 and 9.2 °C warming targets. Lines mark the median and shading marks the 90 % range of the ensemble. c) Atlantic meridional overturning is the maximum of the Atlantic and d) Indo-Pacific meridional overturning is the minimum of the Indo-Pacific meridional overturning streamfunction below 400 m depth. e)  $O_{2sol}$  is the explicitly traced solubility component of oceanic oxygen. i) Oxygen-poor waters are taken as the volume of water with  $O_2 < 50 \text{ mmol m}^{-3}$ .

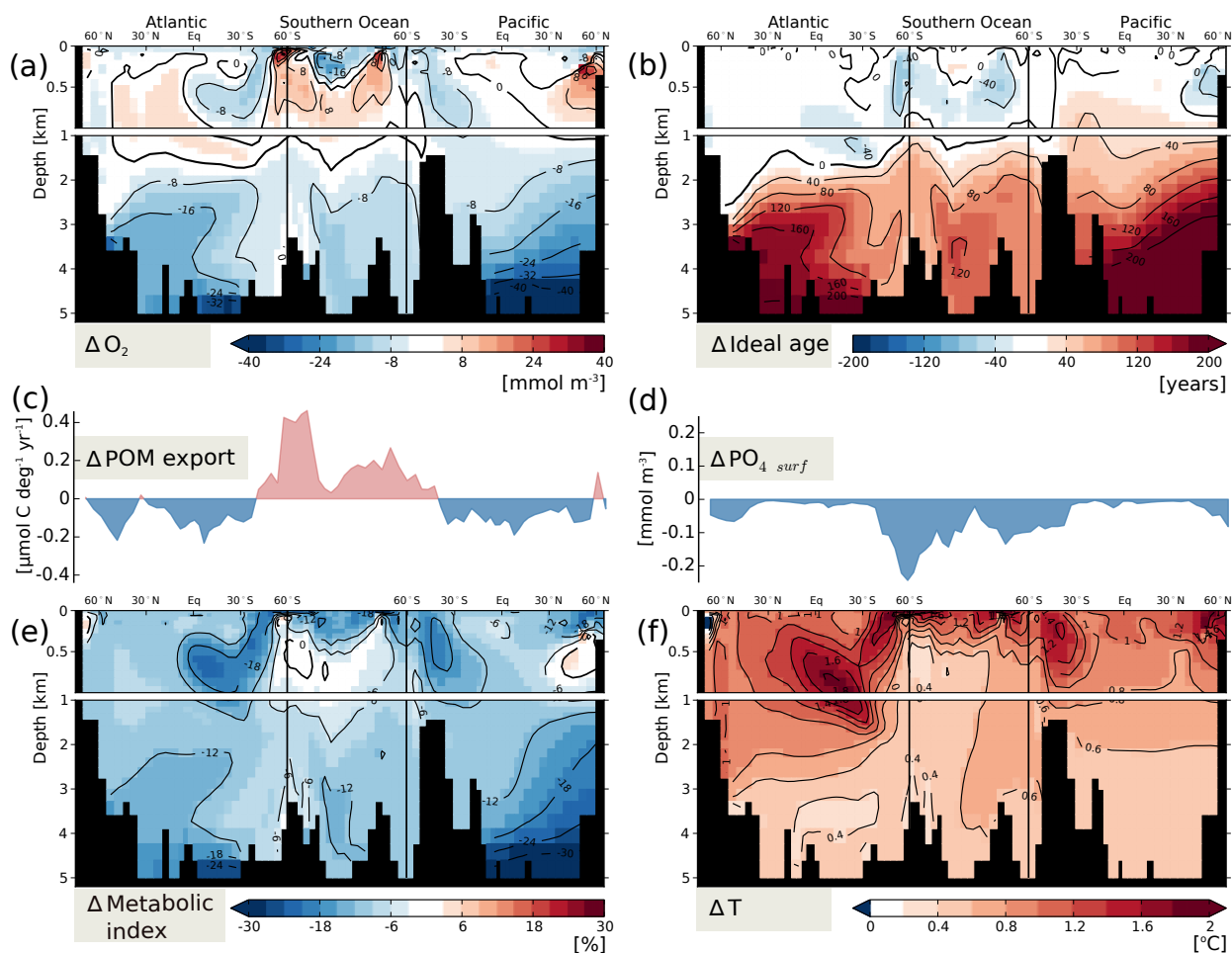


**Figure 3.** Changes in potential ecosystem stressors (a,c,e,f) at peak  $O_2$  decline (AD 3150) relative to preindustrial steady state for a single, representative ensemble member reaching a 1.5 °C warming target. Results are displayed for a cross section through the Atlantic (25° W), across the Southern Ocean (58° S) and into the Pacific (175° W). Changes in ideal age (b) correlate strongly with changes in oxygen (a). Changes in POM export at 75 m (c) and in surface  $PO_4$  concentrations (d) are displayed through the same section.



## 5 Uncertainties in O<sub>2</sub> projections - including a paleo perspective

The pattern and magnitude of global O<sub>2</sub> changes are determined by the response of the overturning circulation. O<sub>2</sub> loss due to less O<sub>2</sub> solubility at higher temperatures gradually decreases oceanic O<sub>2</sub>, in addition. In Bern3D, strong deoxygenation in all basins is projected to peak long after the end of the 21st century, after year AD 3000 and new steady state conditions establish after AD 8000. The equilibration timescale of oceanic oxygen is therefore longer than the thermal equilibration timescale of both the atmosphere (~1000 years) and the ocean (~4000 years). Only few multi-millennial simulations with GCMs currently exist. The response of the overturning circulation on long timescales differs among available model simulations (including EMICs and GCMs) and Bern3D shows a comparatively strong reduction in Indo-Pacific overturning. Uncertainties in the equilibrium climate sensitivity additionally impact projections of O<sub>2</sub> loss due to solubility. These uncertainties directly impact projections of oceanic oxygen.

Similar circulation dynamics as simulated here (Fig. 2c,d) were found by *Rugenstein et al.* (2016) based on EMIC simulations (ECBILT-CLIO) over 10,000 years. *Schmittner et al.* (2008), too, found similar AMOC and Indo-Pacific MOC characteristics for their EMIC (UVic 2.7) over a 2000 year simulation. *Yamamoto et al.* (2015), on the other hand, found different overturning characteristics in a GCM simulation (MIROC 3.2 for a 4xCO<sub>2</sub>) over 2000 years. There AMOC slowed down with no recovery, while AABW decreased only slightly and gradually increased thereafter. Predictions of AMOC have received more attention so far, and AMOC slowdown and partial or full recovery emerges in other multi-millennial simulations (*Zickfeld et al.*, 2013; *Li et al.*, 2013; *Weaver et al.*, 2012). AMOC and Southern Ocean overturning in CMIP5 models was analyzed by *Heuzé et al.* (2015). They found AMOC and Southern Ocean overturning is positively correlated in most CMIP5 models by the end of the 21st century. Generally, preindustrial circulation states, magnitudes and timing of changes are highly model and scenario dependent such that the long-term evolution of meridional overturning is uncertain. As oxygen changes are dominated by circulation changes, this makes the oxygen prediction highly model and scenario dependent, as well. The simulated timing and strength of peak O<sub>2</sub> decrease in Bern3D is similar to what *Schmittner et al.* (2008, AD 3000, 30 % for SRES A2 high emission scenario/SAT~10 °C in Uvic 2.7) found. Other comparable simulations show earlier peaks and smaller magnitudes (*Mathesius et al.* (2015, AD 2600, 16 % decrease for RCP8.5/ΔSAT~7 °C in CLIMBER-3α), *Yamamoto et al.* (2015, after 800 model years, 10 % for 4xCO<sub>2</sub>/ΔSAT~8.5 °C in MIROC 3.2).

Paleo proxies suggest oceanic oxygen concentrations have undergone large climate-driven changes in the past (*Jaccard et al.*, 2014; *Jaccard and Galbraith*, 2012). The deglacial warming of about 3 to 4 °C from the Last Glacial Maximum to the Holocene (*Shakun et al.*, 2012), for instance, has led to oxygenation of the oceans (*Jaccard et al.*, 2014) similar to our model simulations producing 1.5 to 3.3 °C warming above preindustrial. Analogies between reconstructed past and simulated future climate change therefore exist for the respective equilibrium states. Trends at the end of the 21st century, however, are opposite to such expectations. Proxies of past ocean oxygenation and ventilation reveal similar structural changes and mechanisms. Increases in overturning from the LGM to the Holocene are thought to have increased deep oxygen levels and higher temperatures are thought to have decreased O<sub>2</sub> in the upper ocean due to less solubility (*Jaccard et al.*, 2014). The process attribution for both paleo proxies and our long term Earth System projections including 1.5 to 3.3 °C warming targets



are therefore similar. For very large radiative forcing and climate change, such as realized in the RCP8.5 scenario, projected ocean oxygen, however, remains below current concentrations even after reaching a new equilibrium. In Bern3D, changes in ventilation generally outweigh changes in remineralization fluxes as actual driver of oxygen changes. For example, oxygen concentrations decrease in the deep ocean of the low latitude and North Pacific despite lower remineralization fluxes there. At intermediate depth, younger water masses and reduced remineralization fluxes contribute to higher O<sub>2</sub> concentrations. This is in contrast to the mechanisms of O<sub>2</sub> changes identified by *Praetorius et al. (2015)* for the last deglacial transition. They postulate abrupt warming triggered expansion of the North Pacific OMZ at intermediate depth through reduced oxygen solubility and increased productivity there. We note, however, that close comparisons across the different climate states and different climate evolutions remain tentative.

Current generation GCMs, such as is the case for Bern3D, have difficulty simulating the current distribution of OMZs due to missing physical processes operating at small spatial scales, such as eddies and zonal jets (*Cocco et al., 2013; Bopp et al., 2013*) or missing biogeochemical characteristics. Large model-data and model-model discrepancies exist (*Bopp et al., 2013*). *Laufkötter et al. (2017)* recently achieved improved representation of OMZs introducing temperature and oxygen dependence of the remineralization profile within a GCM (GFDL ESM2M). In our ensemble, the magnitude of peak increases in low O<sub>2</sub> waters depend strongly on the rate of organic matter remineralization. Temperature dependent feedback mechanisms, neglected here, may be addressed in future studies. Both particulate sinking speed and local remineralization rates, which control the remineralization profile, have been shown to be sensitive to temperature. While higher temperatures increase bacterial activity and therefore remineralization (*Bendtsen et al., 2014*) they decrease viscosity and therefore increase sinking speed (*Taucher et al., 2014*). The net effect on the remineralization profile is correspondingly uncertain. In addition, ecosystem structure influences the size and density of organic particles available for export (*Armstrong et al., 2001, 2009*). Given these existing uncertainties and the coarse resolution physical models, the projections of OMZs has to be viewed with caution. The general sense of change, that low O<sub>2</sub> waters expand with warmer equilibrium climate states as inferred from proxy observations (*Jaccard et al., 2014*) is not simulated by the ensembles reaching 1.5 and 3.3 °C warming targets. Despite simulated lower background concentrations of O<sub>2</sub> in the subsurface ocean, the volumes of low O<sub>2</sub> waters decrease for steady state conditions in the model. It remains to be explored whether this difference is related to deficiencies in the ocean model or in proxy data or related to the different climate states covered by the proxy data (last glacial termination) and the model simulations.

## 6 Conclusion

Based on CMIP5 models, *Sweetman et al. (2017)* discuss the deep-sea ecosystem implications of climate change by 2100. Deep sea ecosystems provide a range of services from habitat provision, nursery grounds, trophic support, refugia to biodiversity (reviewed in *Sweetman et al., 2017*). Biogeochemical changes such as deoxygenation, warming, acidification and less food availability will likely be accompanied by exploitation of mineral resources, over fishing and dumping of pollutants. We project largest biogeochemical changes beyond 2100 and to aggravate over millennia. How these changes will affect deep-sea



ecosystems is poorly understood. The adaptation to stress may be limited by slow growth rates and long generation times of deep sea ecosystems (*Sweetman et al.*, 2017).

Figure 4a contrasts transient and peak changes in measures of metabolically viable habitats in the upper ocean, hypoxia, and food availability as projected by Bern3D for a 1.5° warmer world. The volume of low oxygen waters is particularly sensitive to anthropogenic warming. While export production, as an indicator of food availability, changes only by some percent, the  
5 volume of water with  $O_2 < 50 \text{ mmol m}^{-3}$  changes by 14 %. Median decreases in the metabolic index, representing viable habitat reductions of the upper ocean, amount to 11 % for a 1.5° warmer world. Higher temperature targets increase the hazard of ecosystem impacts as expressed in the chosen variables. In particular, measures of peak hypoxia exhibit a strong sensitivity to additional warming (Fig. 4b).

Projected peak losses in global mean  $O_2$  scale linearly with forcing such that more stringent mitigation measures would help  
10 to reduce peak  $O_2$  loss by 4.4 %  $^{\circ}\text{C}^{-1}$  of avoided equilibrium warming. At peak  $O_2$  loss, deep-sea environments are projected to be prone to largest changes: Large  $O_2$  loss and slight warming contribute to less metabolic viability. Potential metabolic benefit from increased  $O_2$  concentrations, which may develop at peak  $O_2$  loss in subsurface waters, are offset by increased temperatures in most places. After transient deoxygenation, the future oceanic oxygen inventory in a 1.5 to 3.3 °C warmer world may well exceed preindustrial conditions. Under new steady state conditions, increased metabolic indices develop in better ventilated  
15 waters of the Southern Ocean and deep Indo-Pacific, despite higher temperatures. Yet, under high anthropogenic emissions and forcings such as projected in the RCP8.5 scenario, the total ocean oxygen inventory and metabolic viability is reduced compared to today.

The Earth system response timescale to climate change spans several millennia such that anthropogenic perturbations to greenhouse-gas concentrations commit the Earth system to long-term, irreversible climate change (*Clark et al.*, 2016). Our  
20 simulations show that the long-term fate of oceanic oxygen is characterized by an initial decline followed by a recovery phase. Peak decline and associated potential adverse ecosystem impacts are projected long after stabilization of radiative forcing in the atmosphere. This adds to the list of long-term Earth System commitments including warming, acidification and sea-level rise assessed elsewhere (*Eby et al.*, 2009; *Lord et al.*, 2016; *Pfister and Stocker*, 2016; *Clark et al.*, 2016). Long-term, multi-millennial perspectives are thus required for a full account of climate-related ocean risks.

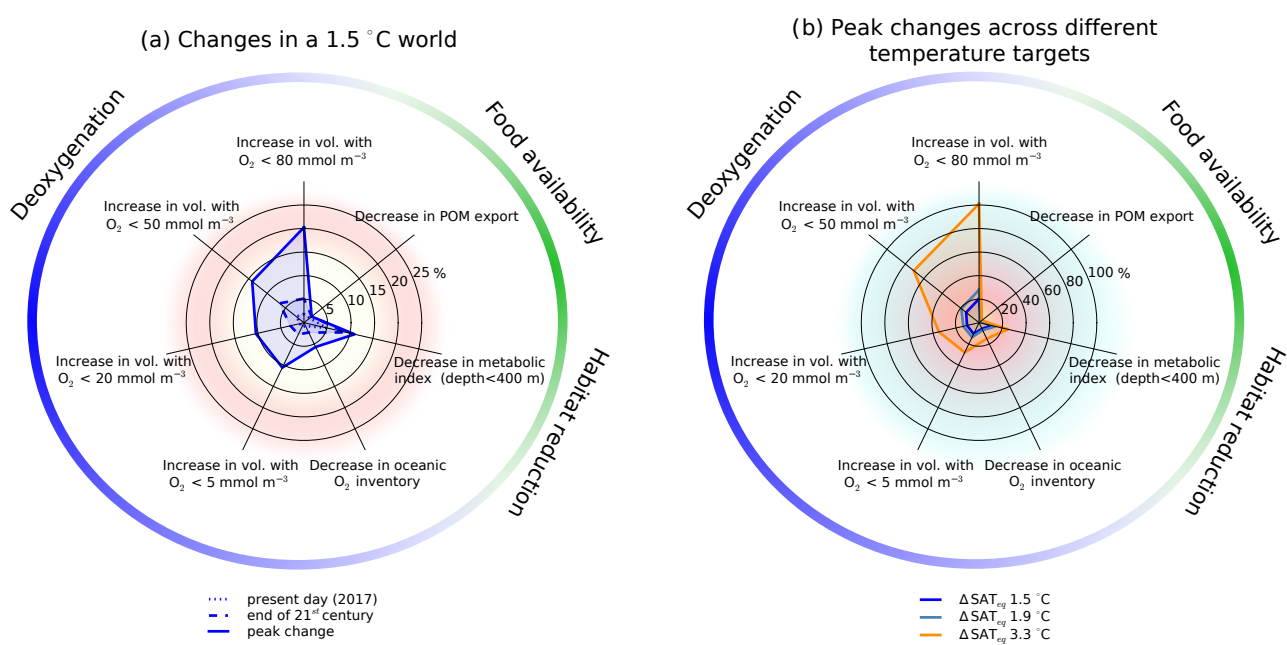


**Figure 4.** Contrasting hazards of ecosystem impacts expressed in measures of hypoxia, metabolic viability of the upper ocean, and food availability. a) Changes for a 1.5 °C warmer world at present, at the end of the century and compared to peak changes. b) Peak changes across 1.5, 1.9 and 3.3 °C temperature targets. Lines correspond to the median response across each ensemble relative to 1870-1899.



25 *Data availability.* Model output is available upon request to the corresponding author ([battaglia@climate.unibe.ch](mailto:battaglia@climate.unibe.ch)).

*Competing interests.* The authors declare that they have no conflict of interest.

*Acknowledgements.* We thank Thomas Frölicher and Andreas Oschlies for fruitful discussions. This work was supported by the Swiss National Science Foundation (200020\_172476).



## References

- Armstrong, R. A., C. Lee, J. I. Hedges, S. Honjo, and S. G. Wakeham (2001), A new, mechanistic model for organic carbon fluxes in the ocean based on the quantitative association of POC with ballast minerals, *Deep Sea Research Part II: Topical Studies in Oceanography*, 49(1), 219–236, doi:10.1016/S0967-0645(01)00101-1, the US JGOFS Synthesis and Modeling Project: Phase 1.
- Armstrong, R. A., M. L. Peterson, C. Lee, and S. G. Wakeham (2009), Settling velocity spectra and the ballast ratio hypothesis, *Deep Sea Research Part II: Topical Studies in Oceanography*, 56(18), 1470–1478, doi:10.1016/j.dsr2.2008.11.032, medFlux:Investigations of Particle Flux in the Twilight Zone.
- Battaglia, G., and F. Joos (2017), Marine N<sub>2</sub>O emissions from nitrification and denitrification constrained by modern observations and projected under large anthropogenic deoxygenation, *Global Biogeochemical Cycles*, in review.
- Battaglia, G., M. Steinacher, and F. Joos (2016), A probabilistic assessment of calcium carbonate export and dissolution in the modern ocean, *Biogeosciences*, 13(9), 2823–2848, doi:10.5194/bg-13-2823-2016.
- Bendtsen, J., K. M. Hilligsøe, J. L. Hansen, and K. Richardson (2014), Analysis of remineralisation, lability, temperature sensitivity and structural composition of organic matter from the upper ocean, *Progress in Oceanography*, doi:10.1016/j.pocean.2014.10.009.
- Bianchi, D., J. P. Dunne, J. L. Sarmiento, and E. D. Galbraith (2012), Data-based estimates of suboxia, denitrification, and N<sub>2</sub>O production in the ocean and their sensitivities to dissolved O<sub>2</sub>, *Global Biogeochem. Cycles*, 26(2), GB2009, doi:10.1029/2011gb004209.
- Bopp, L., C. Le Quéré, M. Heimann, A. C. Manning, and P. Monfray (2002), Climate-induced oceanic oxygen fluxes: Implications for the contemporary carbon budget, *Global Biogeochemical Cycles*, 16(2), 6–16–13.
- Bopp, L., L. Resplandy, J. C. Orr, S. C. Doney, J. P. Dunne, M. Gehlen, P. Halloran, C. Heinze, T. Ilyina, R. Séférian, J. Tjiputra, and M. Vichi (2013), Multiple stressors of ocean ecosystems in the 21st century: projections with CMIP5 models, *Biogeosciences*, 10(10), 6225–6245, doi:10.5194/bg-10-6225-2013.
- Cabre, A., I. Marinov, R. Bernardello, and D. Bianchi (2015), Oxygen minimum zones in the tropical Pacific across CMIP5 models: Mean state differences and climate change trends, *Biogeosciences*, 12(18), 5429–5454, doi:10.5194/bg-12-5429-2015.
- Cheung, W. W. L., G. Reygondeau, and T. L. Frölicher (2016), Large benefits to marine fisheries of meeting the 1.5°C global warming target, *Science*, 354(6319), 1591–1594, doi:10.1126/science.aag2331.
- Clark, P. U., J. D. Shakun, S. A. Marcott, A. C. Mix, M. Eby, S. Kulp, A. Levermann, G. A. Milne, P. L. Pfister, B. D. Santer, D. P. Schrag, S. Solomon, T. F. Stocker, B. H. Strauss, A. J. Weaver, R. Winkelmann, D. Archer, E. Bard, A. Goldner, K. Lambeck, R. T. Pierrehumbert, and G.-K. Plattner (2016), Consequences of twenty-first-century policy for multi-millennial climate and sea-level change, *Nature Climate Change*, 6(4), 360–369, doi:10.1038/nclimate2923.
- Cocco, V., F. Joos, M. Steinacher, T. L. Frölicher, L. Bopp, J. Dunne, M. Gehlen, C. Heinze, J. Orr, A. Oeschlies, B. Schneider, J. Segschneider, and J. Tjiputra (2013), Oxygen and indicators of stress for marine life in multi-model global warming projections, *Biogeosciences*, 10(3), 1849–1868, doi:10.5194/bg-10-1849-2013.
- Deutsch, C., A. Ferrel, B. Seibel, H.-O. Pörtner, and R. B. Huey (2015), Climate change tightens a metabolic constraint on marine habitats, *Science*, 348(6239), 1132–1135, doi:10.1126/science.aaa1605.
- Diaz, R. J., and R. Rosenberg (2008), Spreading Dead Zones and Consequences for Marine Ecosystems, *Science*, 321(5891), 926–929, doi:10.1126/science.1156401.
- Doney, S. C., K. Lindsay, I. Fung, and J. John (2006), Natural Variability in a Stable, 1000-yr Global Coupled Climate–Carbon Cycle Simulation, *J. Climate*, 19(13), 3033–3054, doi:10.1175/JCLI3783.1.



- Eby, M., K. Zickfeld, A. Montenegro, D. Archer, K. J. Meissner, and A. J. Weaver (2009), Lifetime of Anthropogenic Climate Change: Millennial Time Scales of Potential CO<sub>2</sub> and Surface Temperature Perturbations, *Journal of Climate*, 22(10), 2501–2511, doi:10.1175/2008JCLI2554.1.
- Ehlert, D., and K. Zickfeld (2017), What determines the warming commitment after cessation of CO<sub>2</sub> emissions?, *Environmental Research Letters*, 12(1), 015,002.
- 5 Frölicher, T. L., F. Joos, G.-K. Plattner, M. Steinacher, and S. C. Doney (2009), Natural variability and anthropogenic trends in oceanic oxygen in a coupled carbon cycle-climate model ensemble, *Global Biogeochem. Cy.*, 23(GB1003), doi:10.1029/2008GB003316.
- Garcia, H. E., R. A. Locarnini, T. P. Boyer, J. I. Antonov, O. K. Baranova, M. M. Zweng, J. R. Reagan, and D. R. Johnson (2014), World Ocean Atlas 2013, Volume 3: Dissolved Oxygen, Apparent Oxygen Utilization, and Oxygen Saturation, *NOAA Atlas NESDIS 75* 75.
- Gattuso, J.-P., A. Magnan, R. Billé, W. W. L. Cheung, E. L. Howes, F. Joos, D. Allemand, L. Bopp, S. R. Cooley, C. M. Eakin, O. Hoegh-  
10 Guldberg, R. P. Kelly, H.-O. Pörtner, A. D. Rogers, J. M. Baxter, D. Laffoley, D. Osborn, A. Rankovic, J. Rochette, U. R. Sumaila, S. Treyer, and C. Turley (2015), Contrasting futures for ocean and society from different anthropogenic CO<sub>2</sub> emissions scenarios, *Science*, 349(6243), doi:10.1126/science.aac4722.
- Golledge, N. R., D. E. Kowalewski, T. R. Naish, R. H. Levy, C. J. Fogwill, and E. G. W. Gasson (2015), The multi-millennial Antarctic commitment to future sea-level rise, *Nature*, 526(7573), 421–425, doi:10.1038/nature15706.
- 15 Gruber, N. (2011), Warming up, turning sour, losing breath: ocean biogeochemistry under global change, *Philos. T. R. Soc. A*, 369(1943), 1980–1996, doi:10.1098/rsta.2011.0003.
- Heuzé, C., K. J. Heywood, D. P. Stevens, and J. K. Ridley (2015), Changes in Global Ocean Bottom Properties and Volume Transports in CMIP5 Models under Climate Change Scenarios, *Journal of Climate*, 28(8), 2917–2944, doi:10.1175/JCLI-D-14-00381.1.
- Ito, T., S. Minobe, M. C. Long, and C. Deutsch (2017), Upper ocean O<sub>2</sub> trends: 1958–2015, *Geophysical Research Letters*, 44(9), 4214–4223.
- 20 Jaccard, S., E. D. Galbraith, T. L. Frölicher, and N. Gruber (2014), Ocean (De)oxygenation Across the Last Deglaciation: Insights for the Future, *Oceanography*, 27.
- Jaccard, S. L., and E. D. Galbraith (2012), Large climate-driven changes of oceanic oxygen concentrations during the last deglaciation, *Nature Geosci*, 5(2), 151–156, doi:10.1038/ngeo1352, 10.1038/ngeo1352.
- Jaccard, S. L., E. D. Galbraith, A. Martínez-García, and R. F. Anderson (2016), Covariation of deep Southern Ocean oxygenation and  
25 atmospheric CO<sub>2</sub> through the last ice age, *Nature*, 530(7589), 207–210.
- Joos, F., and R. Spahni (2008), Rates of change in natural and anthropogenic radiative forcing over the past 20,000 years, *P. Natl. Acad. Sci. USA*, 105(5), 1425–1430, doi:10.1073/pnas.0707386105.
- Kalnay, E., M. Kanamitsu, R. Kistler, W. Collins, D. Deaven, L. Gandin, M. Iredell, S. Saha, G. White, J. Woollen, Y. Zhu, M. Chelliah, W. Ebisuzaki, W. Higgins, J. Janowiak, K. C. Mo, C. Ropelewski, J. Wang, A. Leetmaa, R. Reynolds, R. Jenne,  
30 and D. Joseph (1996), The NCEP/NCAR 40-year reanalysis project, *B. Am. Meteorol. Soc.*, 77(3), 437–471, doi:10.1175/1520-0477(1996)077<0437:TNYRP>2.0.CO;2.
- Keeling, R. F., A. Körtzinger, and N. Gruber (2010), Ocean Deoxygenation in a Warming World, *Annual review of marine science*, 2, 199–229.
- Key, R. M., A. Kozyr, C. L. Sabine, K. Lee, R. Wanninkhof, J. L. Bullister, R. A. Feely, F. J. Millero, C. Mordy, and T.-H. Peng (2004),  
35 A global ocean carbon climatology: Results from Global Data Analysis Project (GLODAP), *Global Biogeochem. Cy.*, 18(4), GB4031, doi:10.1029/2004GB002247.



- Laufkötter, C., J. G. John, C. A. Stock, and J. P. Dunne (2017), Temperature and oxygen dependence of the remineralization of organic matter, *Global Biogeochemical Cycles*, doi:10.1002/2017GB005643, 2017GB005643.
- Li, C., J.-S. von Storch, and J. Marotzke (2013), Deep-ocean heat uptake and equilibrium climate response, *Climate Dynamics*, 40(5), 1071–1086, doi:10.1007/s00382-012-1350-z.
- Lord, N. S., A. Ridgwell, M. C. Thorne, and D. J. Lunt (2016), An impulse response function for the “long tail” of excess atmospheric CO<sub>2</sub> in an Earth system model, *Global Biogeochemical Cycles*, 30(1), 2–17, doi:10.1002/2014GB005074, 2014GB005074.
- Magnan, A. K., M. Colombier, R. Billé, F. Joos, O. Hoegh-Guldberg, H.-O. Pörtner, H. Waisman, T. Spencer, and J.-P. Gattuso (2016), Implications of the Paris agreement for the ocean, *Nature Climate Change*, 6(8), 732–735, doi:10.1038/nclimate3038.
- Martin, J. H., G. A. Knauer, D. M. Karl, and W. Broenkow (1987), VERTEX: Carbon cycling in the northeast Pacific, *Deep-Sea Res.*, doi:10.1016/0198-0149(87)90086-0.
- 10 Matear, R. J. (2000), Climate change impacts on marine systems, *Aust. Microbiol.*, 21(2), 17 – 20.
- Matear, R. J., and A. C. Hirst (2003), Long-term changes in dissolved oxygen concentrations in the ocean caused by protracted global warming, *Global Biogeochemical Cycles*, 17(4), doi:10.1029/2002GB001997, 1125.
- Mathesius, S., M. Hofmann, K. Caldeira, and J. Schellnhuber Hans (2015), Long-term response of oceans to CO<sub>2</sub> removal from the atmosphere, *Nature Clim. Change*, 5(12), 1107–1113.
- 15 McKay, M. D., R. J. Beckman, and W. J. Conover (1979), A comparison of three methods for selecting values of input variables in the analysis of output from a computer code, *Technometrics*, 21, 239–245.
- Meinshausen, M., S. Smith, K. Calvin, J. Daniel, M. Kainuma, J.-F. Lamarque, K. Matsumoto, S. Montzka, S. Raper, K. Riahi, A. Thomson, G. Velders, and D. P. van Vuuren (2011), The RCP greenhouse gas concentrations and their extensions from 1765 to 2300, *Climatic Change*, 109(1), 213–241, doi:10.1007/s10584-011-0156-z.
- 20 Mislan, K. A. S., C. A. Deutsch, R. W. Brill, J. P. Dunne, and J. L. Sarmiento (2017), Projections of climate-driven changes in tuna vertical habitat based on species-specific differences in blood oxygen affinity, *Global Change Biology*, 23(10), 4019–4028, doi:10.1111/gcb.13799.
- Müller, S. A., F. Joos, N. R. Edwards, and T. F. Stocker (2006), Water mass distribution and ventilation time scales in a cost-efficient, three-dimensional ocean model, *J. Climate*, 19(21), 5479–5499, doi:10.1175/JCLI3911.1.
- Müller, S. A., F. Joos, N. R. Edwards, and T. F. Stocker (2008), Modeled natural and excess radiocarbon: Sensitivities to the gas exchange formulation and ocean transport strength, *Global Biogeochem. Cy.*, 22(GB3011), 14 pp, doi:10.1029/2007GB003065.
- 25 Najjar, R. G., J. Orr, C. L. Sabine, and F. Joos (1999), Biotic-HOWTO. Internal OCMIP Report, *Tech. rep.*, LSCE/CEA Saclay, Gif-sur-Yvette, France.
- Orr, J., and R. G. Najjar (1999), Abiotic-HOWTO. Internal OCMIP Report, *Tech. rep.*, LSCE/CEA Saclay, Gif-sur-Yvette, France.
- Orr, J. C., and J.-M. Epitalon (2015), Improved routines to model the ocean carbonate system: mocsy 2.0, *Geoscientific Model Development*, 8(3), 485–499, doi:10.5194/gmd-8-485-2015.
- 30 Oschlies, A., O. Duteil, J. Getzlaff, W. Koeve, A. Landolfi, and S. Schmidtko (2017), Patterns of deoxygenation: sensitivity to natural and anthropogenic drivers, *Philosophical Transactions of the Royal Society of London A: Mathematical, Physical and Engineering Sciences*, 375(2102), doi:10.1098/rsta.2016.0325.
- Parekh, P., F. Joos, and S. A. Müller (2008), A modeling assessment of the interplay between aeolian iron fluxes and iron-binding ligands in controlling carbon dioxide fluctuations during Antarctic warm events, *Paleoceanography*, 23, PA4202, doi:10.1029/2007PA001531.
- 35 Pfister, P. L., and T. F. Stocker (2016), Earth system commitments due to delayed mitigation, *Environmental Research Letters*, 11(1), 014,010.



- Plattner, G.-K., F. Joos, T. F. Stocker, and O. Marchal (2001), Feedback mechanisms and sensitivities of ocean carbon uptake under global warming, *Tellus B*, 53(5), 564–592, doi:10.1034/j.1600-0889.2001.530504.x.
- Plattner, G.-K., R. Knutti, F. Joos, T. F. Stocker, W. von Bloh, V. Brovkin, D. Cameron, E. Driesschaert, S. Dutkiewicz, M. Eby, N. R. Edwards, T. Fichfet, J. C. Hargreaves, C. D. Jones, M. F. Loutre, H. D. Matthews, a. Mouchet, S. a. Müller, S. Nawrath, a. Price, a. Sokolov, K. M. Strassmann, and a. J. Weaver (2008), Long-Term Climate Commitments Projected with Climate–Carbon Cycle Models, *Journal of Climate*, 21(12), 2721–2751, doi:10.1175/2007JCLI1905.1.
- 5 Pörtner, H.-O. (2010), Oxygen- and capacity-limitation of thermal tolerance: a matrix for integrating climate-related stressor effects in marine ecosystems, *Journal of Experimental Biology*, 213(6), 881–893, doi:10.1242/jeb.037523.
- Praetorius, S. K., A. C. Mix, M. H. Walczak, M. D. Wolhowe, J. A. Addison, and F. G. Prahl (2015), North Pacific deglacial hypoxic events linked to abrupt ocean warming, *Nature*, 527(7578), 362–366.
- 10 Ritz, S. P., T. F. Stocker, and F. Joos (2011), A coupled dynamical ocean-energy balance atmosphere model for paleoclimate studies, *J. Climate*, 24(2), 349–375, doi:10.1175/2010JCLI3351.1.
- Roth, R., S. P. Ritz, and F. Joos (2014), Burial-nutrient feedbacks amplify the sensitivity of carbon dioxide to changes in organic matter remineralisation, *Earth System Dynamics*, 5(1), 321–343, doi:10.5194/esdd-5-473-2014.
- Rugenstein, M. A. A., J. Sedláček, and R. Knutti (2016), Nonlinearities in patterns of long-term ocean warming, *Geophysical Research Letters*, 43(7), 3380–3388, doi:10.1002/2016GL068041, 2016GL068041.
- 15 Schmidtko, S., L. Stramma, and M. Visbeck (2017), Decline in global oceanic oxygen content during the past five decades, *Nature*, 542(7641), 335–339, doi:10.1038/nature21399.
- Schmittner, A., A. Oschlies, H. D. Matthews, and E. D. Galbraith (2008), Future changes in climate, ocean circulation, ecosystems, and biogeochemical cycling simulated for a business-as-usual CO<sub>2</sub> emission scenario until year 4000 AD, *Global Biogeochem. Cy.*, 22(1), GB1013—, doi:10.1029/2007GB002953.
- 20 Shakun, J. D., P. U. Clark, F. He, S. A. Marcott, A. C. Mix, Z. Liu, B. Otto-Bliesner, A. Schmittner, and E. Bard (2012), Global warming preceded by increasing carbon dioxide concentrations during the last deglaciation, *Nature*, 484(7392), 49–54, doi:10.1038/nature10915.
- Steinacher, M., F. Joos, L. Bopp, P. Cadule, S. C. Doney, M. Gehlen, B. Schneider, and J. Segschneider (2009), Projected 21st century decrease in marine productivity : a multi-model analysis, pp. 7933–7981.
- 25 Storch, D., L. Menzel, S. Frickenhaus, and H. O. Pörtner (2014), Climate sensitivity across marine domains of life: limits to evolutionary adaptation shape species interactions, *Global Change Biology*, 20(10), 3059–3067.
- Sweetman, A. K., A. Thurber, C. Smith, L. Levin, C. Mora, and C. L. Wei (2017), Major impacts of climate change on deep-sea benthic ecosystems, *Elem Sci Anth*, 5:4.
- Taucher, J., L. T. Bach, U. Riebesell, and A. Oschlies (2014), The viscosity effect on marine particle flux: A climate relevant feedback mechanism, *Global Biogeochemical Cycles*, 28(4), 415–422, 2013GB004728.
- 30 Tschumi, T., F. Joos, M. Gehlen, and C. Heinze (2011), Deep ocean ventilation, carbon isotopes, marine sedimentation and the deglacial CO<sub>2</sub> rise, *Clim. Past*, 7(3), 771–800, doi:10.5194/cp-7-771-2011.
- UNFCCC (accessed 11. October 2017), Adoption of The Paris Agreement, [http://unfccc.int/paris\\_agreement/items/9485.php](http://unfccc.int/paris_agreement/items/9485.php).
- Weaver, A. J., J. Sedláček, M. Eby, K. Alexander, E. Crespin, T. Fichfet, G. Philippon-Berthier, F. Joos, M. Kawamiya, K. Matsumoto, M. Steinacher, K. Tachiiri, K. Tokos, M. Yoshimori, and K. Zickfeld (2012), Stability of the Atlantic meridional overturning circulation: A model intercomparison, *Geophysical Research Letters*, 39(20).
- 35 Weiss, R. (1974), Carbon dioxide in water and seawater: The solubility of a non-ideal gas, *Mar. Chem.*, 2, 203–215.



- Winkelmann, R., A. Levermann, A. Ridgwell, and K. Caldeira (2015), Combustion of available fossil fuel resources sufficient to eliminate the Antarctic Ice Sheet, *Science Advances*, 1(8), doi:10.1126/sciadv.1500589.
- Yamamoto, A., A. Abe-Ouchi, M. Shigemitsu, A. Oka, K. Takahashi, R. Ohgaito, and Y. Yamanaka (2015), Global deep ocean oxygenation by enhanced ventilation in the Southern Ocean under long-term global warming, *Global Biogeochemical Cycles*, 29(10), 1801–1815, doi:10.1002/2015GB005181, 2015GB005181.
- 5 Zickfeld, K., M. Eby, A. J. Weaver, K. Alexander, E. Crespín, N. R. Edwards, A. V. Eliseev, G. Feulner, T. Fichefet, C. E. Forest, P. Friedlingstein, H. Goosse, P. B. Holden, F. Joos, M. Kawamiya, D. Kicklighter, H. Kienert, K. Matsumoto, I. I. Mokhov, E. Monier, S. M. Olsen, J. O. P. Pedersen, M. Perrette, G. Philippon-Berthier, A. Ridgwell, A. Schlosser, T. S. V. Deimling, G. Shaffer, A. Sokolov, R. Spahni, M. Steinacher, K. Tachiiri, K. S. Tokos, M. Yoshimori, N. Zeng, and F. Zhao (2013), Long-Term Climate Change Commitment and Reversibility: An EMIC Intercomparison, *Journal of Climate*, 26(16), 5782–5809, doi:10.1175/JCLI-D-12-00584.1.
- 10 Zickfeld, K., S. Solomon, and D. M. Gilford (2017), Centuries of thermal sea-level rise due to anthropogenic emissions of short-lived greenhouse gases, *Proceedings of the National Academy of Sciences*, 114(4), 657–662.